Enhancement of the spin Hall angle by quantum confinement

Christian Herschbach,[1,2,*] Martin Gradhand,[3] Dmitry V. Fedorov,[1,2] and Ingrid Mertig[1,2]

[1]*Max Planck Institute of Microstructure Physics, Weinberg 2, 06120 Halle, Germany*
[2]*Institute of Physics, Martin Luther University Halle-Wittenberg, 06099 Halle, Germany*
[3]*H.H. Wills Physics Laboratory, University of Bristol, Bristol BS8 1TH, United Kingdom*

We present *ab initio* calculations of the skew-scattering contribution to the spin Hall effect for freestanding fcc Au(111) films. Their thickness is varied between 1 and 32 monolayers, and Pt atoms are considered as substitutional impurities and adatoms. The obtained spin Hall angle drastically changes with varying impurity positions in the film. Impurities in the adatom position play a special role reversing sign of the spin Hall angle. In addition, we show that Pt adatoms on one-monolayer noble metal films cause a *gigantic* spin Hall angle up to 18%, which is attributed to the lack of interband transitions.

I. INTRODUCTION

For practical applications of the spin Hall effect (SHE) in spintronics devices it is of crucial importance to identify materials with a large spin Hall angle (SHA). This quantity indicates the efficiency of charge to spin current conversion. After the first measurement of the *gigantic* SHE in Au,[1] with a SHA of about 11%, an intensive discussion about responsible mechanisms started.[2–5] Recent experiments with Pt-doped Au films found a comparable large SHA.[6] Therefore, theoretical investigations of the influence of reduced dimension on the SHA are highly desirable. In this paper we present an *ab initio* study of the SHE for freestanding fcc Au(111) films of varying thicknesses. We concentrate on the skew-scattering mechanism which is shown to be dominant for dilute alloys with impurity concentrations less than a few at.%.[7–10]

II. METHOD

Our calculations are based on density-functional theory solving the Dirac equation by means of a relativistic screened Korringa-Kohn-Rostoker (KKR) Green's function method, as explained in detail in Refs. 11 and 12. To perform transport calculations, we solve the linearized Boltzmann equation for the vector mean free path

$$\Lambda_{\mathbf{k}}^m = \tau_{\mathbf{k}}^m \left(\mathbf{v}_{\mathbf{k}}^m + \sum_{\mathbf{k}'m'} P_{\mathbf{k}'\mathbf{k}}^{m'm} \Lambda_{\mathbf{k}'}^{m'} \right) \quad (1)$$

iteratively.[13] Here, $\tau_{\mathbf{k}}^m = (\sum_{\mathbf{k}'m'} P_{\mathbf{k}\mathbf{k}'}^{mm'})^{-1}$ is the relaxation time and $\mathbf{v}_{\mathbf{k}}^m$ denotes the group velocity corresponding to the crystal momentum $\mathbf{k}$ and the spin-resolved band m. The latter one is a combined index, $m = \{n, \sigma\}$, since for nonmagnetic systems with inversion symmetry, each band n is twofold degenerate with respect to the relativistic spin state labeled by $\sigma = \{+, -\}$.[12] An important point in Eq. (1) is the presence of the *scattering-in* term $\sim \sum_{\mathbf{k}'m'} P_{\mathbf{k}'\mathbf{k}}^{m'm} \Lambda_{\mathbf{k}'}^{m'}$, shown to be mandatory for the SHE.[4] The sums above incorporate spin-conserving as well as spin-flip scattering processes.

The microscopic transition probability $P_{\mathbf{k}\mathbf{k}'}^{mm'}$ can be expressed in the dilute limit of impurity concentration c_0 (with the number of impurities $c_0 N$) as[13]

$$P_{\mathbf{k}\mathbf{k}'}^{mm'} = \frac{2\pi}{\hbar} c_0 N \left| T_{\mathbf{k}\mathbf{k}'}^{mm'} \right|^2 \delta\left(E_{\mathbf{k}}^m - E_{\mathbf{k}'}^{m'} \right). \quad (2)$$

The corresponding transition matrix elements $T_{\mathbf{k}\mathbf{k}'}^{mm'}$ are calculated from the self-consistent solution of the impurity problem via Dyson and Lippmann-Schwinger equations.[4] It takes into account charge relaxation around the impurity on a real-space cluster of four nearest-neighbor shells.

The conductivity tensor can be expressed in the low-temperature limit as a Fermi-surface integral.[4,13] In the case of a two-dimensional (2D) system, it is reduced to a sum of Fermi-line integrals[14]

$$\underline{\sigma} = \frac{e^2}{\hbar (2\pi)^2 d} \sum_m \oint_{E_{\mathbf{k}}=E_F} \frac{dl_m}{|\mathbf{v}_{\mathbf{k}}^m|} \mathbf{v}_{\mathbf{k}}^m \circ \Lambda_{\mathbf{k}}^m, \quad (3)$$

where d is the film thickness. Thus, only electrons at the Fermi level (E_F) contribute to transport. For the spin conductivity tensor[4]

$$\underline{\sigma}^s = \frac{e^2}{\hbar (2\pi)^2 d} \sum_m \oint_{E_{\mathbf{k}}=E_F} \frac{dl_m}{|\mathbf{v}_{\mathbf{k}}^m|} s_z^m(\mathbf{k}) \mathbf{v}_{\mathbf{k}}^m \circ \Lambda_{\mathbf{k}}^m, \quad (4)$$

the spin polarization $s_z^m(\mathbf{k}) = \langle \Psi_{m\mathbf{k}} | \hat{\beta} \hat{\sigma}_z | \Psi_{m\mathbf{k}} \rangle$ (Ref. 12) is included. A decomposition of $\underline{\sigma}^s$ into the band- and $\mathbf{k}$-resolved contributions, $\underline{\sigma}_n^s$ and $\underline{\sigma}_n^s(\mathbf{k})$, by

$$\underline{\sigma}^s = \sum_{m(n,\sigma)} \underline{\sigma}_m^s = \sum_n \underline{\sigma}_n^s = \sum_n \oint_{E_{\mathbf{k}}=E_F} dl_n \, \underline{\sigma}_n^s(\mathbf{k}), \quad (5)$$

offers insight into the microscopic origin of the phenomenon. As a consequence of the 2D geometry, the Bloch vector has only two in-plane components, $\mathbf{k} = (k_x, k_y, 0)$, if the z axis is chosen along the growth direction of the film. The same holds for $\mathbf{v}_{\mathbf{k}}^m$ and $\Lambda_{\mathbf{k}}^m$.

To quantify the strength of the SHE, commonly the spin Hall angle

$$\alpha = \sigma_{yx}^s / \sigma_{xx} \quad (6)$$

is used. It is the ratio of the spin Hall conductivity (SHC) σ_{yx}^s to the longitudinal charge conductivity σ_{xx}.[4] Both quantities depend inversely on the impurity concentration c_0. Thus, α

is concentration independent. Therefore, the SHA is a very useful quantity for comparison with experiment.

The main focus of this paper is the investigation of the influence of delta doping on the SHA. In other words, we study α as a function of impurity position within the film. For the considered Au films, all twofold-degenerate subbands n stem from one and the same spin-degenerate bulk band. Thus, the subband index n can be mapped onto the bulk quantum number k_z.[15,16] As a consequence, each subband state can be considered as a superposition of two bulk states with k_z and $-k_z$ forming a standing wave in growth direction of the film. Since Au has a simple single-sheeted Fermi surface, there are no degeneracies between different subbands. In this particular case an electron state can be uniquely characterized by **k** and σ omitting n for simplicity.

III. RESULTS

The main result of our calculations is depicted in Fig. 1, where the SHA is shown as a function of the Pt impurity position for different Au film thicknesses. Several conclusions can be drawn. First, α changes sign for Pt adatoms with respect to substitutional impurities within the film. This is valid for all systems under consideration, except for the 2 ML film, which will be discussed later. Second, α varies strongly as a function of impurity position. The magnitude of the SHA does not, however, exceed the corresponding bulk value of 1%,[4] besides for the 1 ML film, where Pt adatoms cause an enhanced $|\alpha|$ up to 13%.

The absolute values of the SHA can be qualitatively understood by the fact that for larger α, stronger scattering is required. Stronger scattering would cause a higher spin Hall conductivity and a decreased longitudinal charge conductivity. According to Eq. (6), this should definitely enlarge the SHA. The influence of quantum confinement can be explained in terms of a quantum well model. Half of the eigenfunctions are antisymmetric with respect to the center of the well,
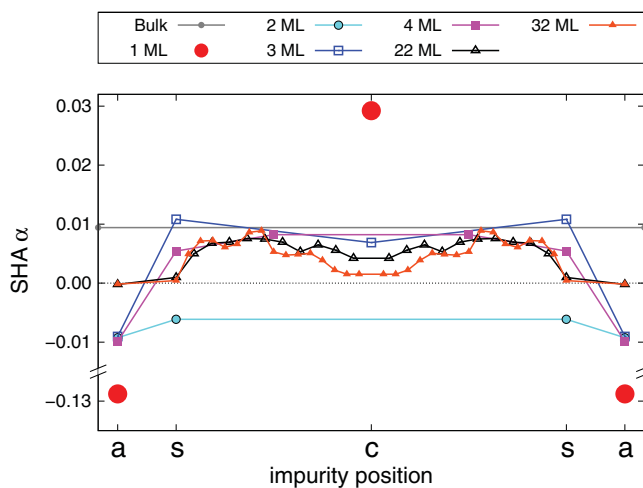
FIG. 1. (Color online) The spin Hall angle α for Au(111) films with varying thicknesses. Pt impurities are considered at several sites within the film shown on a normalized abscissa fixing adatom "a", surface layer "s", and central layer "c" positions. The lines are to guide the eyes.

where they have a node, and all solutions vanish at the boundaries.[17] Therefore, impurities at the central position or at the boundaries cause weaker scattering than impurities elsewhere and the SHA is reduced. This is reflected in our calculations for thicker films (see Fig. 1). In the case of thin films, their thickness becomes comparable to the size of the scattering region. As a consequence, the perturbation of the potential extends over the whole film without localization at a certain node. This results in stronger scattering and a larger SHA.

In order to understand the sign of α, we analyzed the **k**-resolved contributions to σ_{yx}^s in terms of the antisymmetric part

$$\sigma_{A,yx}^s(\mathbf{k}) = \tfrac{1}{2}\{\underline{\sigma}^s(\mathbf{k}) - [\underline{\sigma}^s(\mathbf{k})]^T\}_{yx}, \qquad (7)$$

of $[\underline{\sigma}^s(\mathbf{k})]_{yx}$, which causes the SHC. Here the superscript T denotes the transpose. The sign of $\sigma_{A,yx}^s(\mathbf{k})$ can be easily obtained within a simple picture. Taking into account Eqs. (4) and (5) and the symmetry relation $s_z^+(\mathbf{k}) = -s_z^-(\mathbf{k})$, one finds $\sigma_{A,yx}^s(\mathbf{k}) \sim [(\Lambda_\mathbf{k}^+ - \Lambda_\mathbf{k}^-) \times \mathbf{v_k}]_z$. Here the group velocity does not have the spin channel index since $\mathbf{v}_\mathbf{k}^+ = \mathbf{v}_\mathbf{k}^-$ holds for degenerate states. The difference $(\Lambda_\mathbf{k}^+ - \Lambda_\mathbf{k}^-)$ represents the spin anisotropy of the mean free path caused by the spin-orbit coupling. Thus, the sign of $\sigma_{A,yx}^s(\mathbf{k})$ is entirely defined by the sign of $\sin(\angle[(\Lambda_\mathbf{k}^+ - \Lambda_\mathbf{k}^-),\mathbf{v_k}])$. This means that $(\Lambda_\mathbf{k}^+ - \Lambda_\mathbf{k}^-)$ pointing into the left half plane of $\mathbf{v_k}$ results in a negative SHA, whereas the opposite is valid for $(\Lambda_\mathbf{k}^+ - \Lambda_\mathbf{k}^-)$ pointing into the right half plane. With Eqs. (1) and (6) it becomes clear that the microscopic transition probability, appearing in the scattering-in term, causes the spin-dependent deviation of $\Lambda_\mathbf{k}^\pm$ from the direction of $\mathbf{v_k}$ and consequently determines the sign of α.

Thus, $\sigma_{A,yx}^s(\mathbf{k})$ offers insight into the microscopic origin of the sign of the SHA. Figure 2 shows the results obtained from Eq. (7) for five different Au film thicknesses. The left and right columns correspond to Pt impurities in the adatom and surface layer position, respectively. In addition, the subband-resolved contributions α_n to the SHA, defined by

$$\alpha = \sum_n \alpha_n = \sum_n \left[\underline{\sigma}_n^s\right]_{yx}\big/\sigma_{xx}, \qquad (8)$$

are given for the thin films. Evidently, only the case of the 1 ML film looks quite trivial with respect to the sign change of the total α. For all the other thicknesses we obtain subband contributions with opposite sign. Nevertheless, the distribution of $\sigma_{A,yx}^s(\mathbf{k})$, constructed according to Eqs. (5) and (7), properly reflects the sign of the subband-resolved SHA shown in Fig. 2.

Furthermore, for a fixed impurity position, Fermi lines in the same region of the Brillouin zone (BZ) show similar behavior with respect to the sign of $\sigma_{A,yx}^s(\mathbf{k})$, independent of the film thickness. This fact is connected to the discussion above. The bulk system has fcc symmetry, whereas the 2D BZ of the film is hexagonal, which determines the symmetry of the Fermi lines. A certain Fermi line can be considered as a superposition of two sections of the bulk Fermi surface corresponding to the related k_z and $-k_z$. The thicker the film, the more Fermi lines appear and sample the bulk Fermi surface. The thinner the film, the less Fermi lines occur and the more pronounced are the quantum size effects, which have strongest impact on the 1 and 2 ML films.
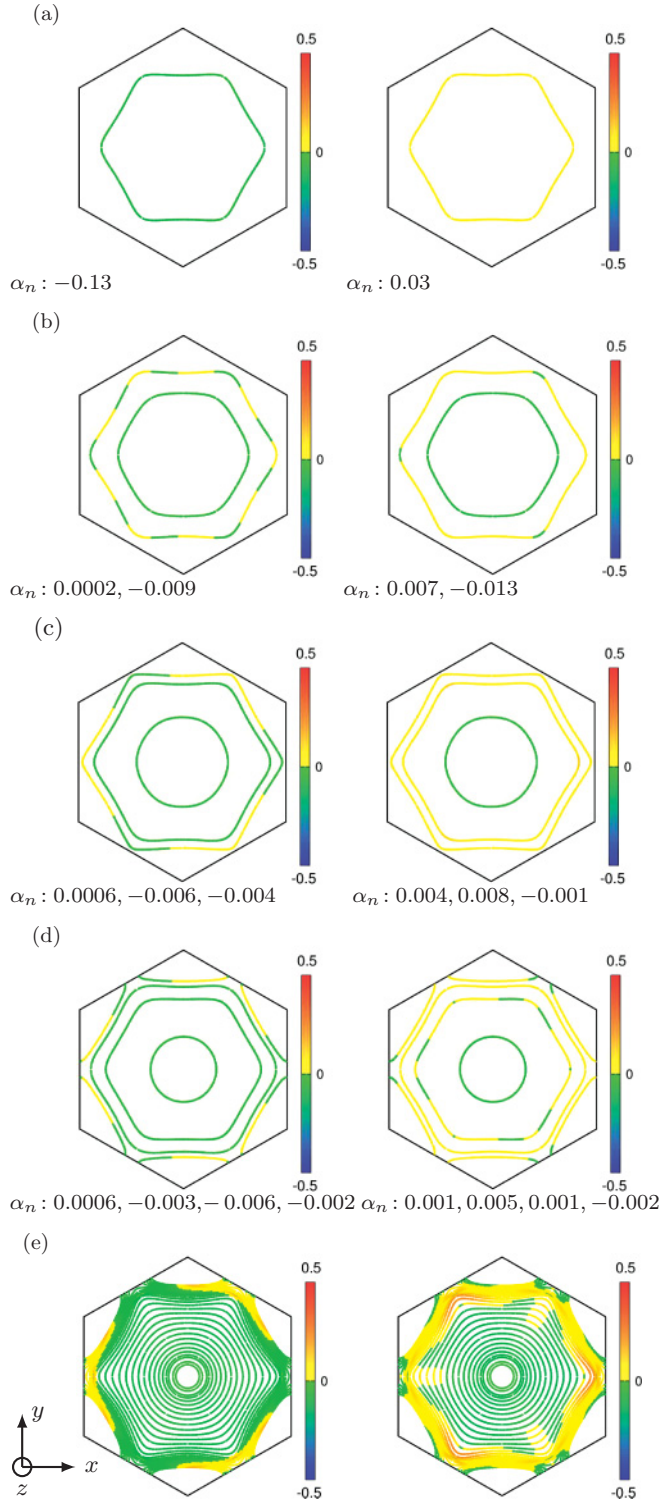
FIG. 2. (Color online) The antisymmetric part $\sigma_{A,yx}^{s}(\mathbf{k})$ of the $\mathbf{k}$-resolved contributions to the SHC (in arbitrary units) for (a) 1 ML, (b) 2 ML, (c) 3 ML, (d) 4 ML, and (e) 32 ML Au(111) films with Pt impurities as adatoms (left) and in the surface layer (right). For the thin films, the subband contributions α_n, going from outer to inner Fermi lines, are given.

To clarify the peculiar situation of the gigantic SHA for 1 ML and its constant sign for the 2 ML system (Fig. 1), we performed auxiliary calculations for Cu and Ag fcc(111)

TABLE I. The spin Hall angle for 1 and 2 ML of Cu, Ag, and Au fcc(111) films with Pt impurities in the adatom ("a") and surface layer ("s") positions.

Host system	Cu	Ag	Au
1 ML "a"	-0.180	-0.182	-0.129
"s"	0.097	0.061	0.029
2 ML "a"	-0.030	-0.035	-0.009
"s"	0.011	0.002	-0.006

films with the same number of monolayers. Table I shows a comparison of the corresponding α for the three hosts. For both thicknesses, one can see a clear trend of decreasing SHA for the impurities in the surface layer position going from Cu to Au. This is in agreement with the results obtained for substitutional Pt impurities in the related bulk noble metals.[18] The reason is the reduced difference between the spin-orbit coupling of the Pt impurity and the replaced host atom going from Cu to Au. The negative sign of α for impurities in the surface layer of the 2 ML Au film can be explained in this context with Fig. 2, right column. One can see that for thicker films only a few Fermi lines show negative contributions. Consequently, the sign of their total SHA is well defined and positive. For the 2 ML film just two subbands appear and contribute with opposite sign to the total α. Which of the contributions is dominating depends on the system. While for the 2 ML Cu and Ag films the sign of the SHA for the surface layer impurity position is positive and provided by the outer Fermi line, the negative sign was obtained for Au due to the dominant contribution from the inner Fermi line.

Now we focus on the 1 ML Au film with Pt adatoms, which provides a SHA of about 13% (Fig. 1). In fact, an enhancement of α for thin films with impurities in the adatom position could be generally expected. The skew-scattering contribution to the SHE is caused by the spin-orbit interaction modulated by impurity atoms.[18] This modulation is particularly large for adatoms since they provide strong potential gradients. However, the gigantic SHA is only obtained for the 1 ML film among all considered thicknesses. Even higher values of α ($\approx$18%) are found for 1 ML Cu and Ag films (Table I), but nothing similar is seen for 2 ML films. Thus, the enhancement of the SHA looks like a particular property of the 1 ML films. To elucidate this phenomenon, we performed additional calculations for several films neglecting interband transitions in Eq. (1). The corresponding results for the SHC for four Au films with Pt adatoms are shown in Table II. Obviously, for each film the SHC is significantly increased, neglecting interband transitions. The same result was found for Cu and Ag films.

TABLE II. Spin Hall conductivity $[(\mu\Omega\,\text{cm})^{-1}]$ for four different thicknesses of Au(111) films with Pt adatoms neglecting and including interband transitions (IT). The impurity density is 1.4×10^{13} cm^{-2} (1 impurity atom per 100 film unit cells).

Film thickness	1 ML	2 ML	3 ML	4 ML
Neglecting IT	-0.095	-0.094	-0.15	-0.046
Including IT	-0.095	-0.0076	-0.0072	-0.0074

The fact of increased SHC without interband scattering is obtained for any impurity position within all the considered films. To understand its physical meaning, one can employ the relation of different subbands labeled by n to the corresponding bulk quantum number k_z. In these terms an interband transition is connected with a certain out-of-plane scattering which reduces σ_{yx}^s.

In agreement with experiment[6] and other calculations[19] our results show an increase of the SHE due to reduced film thickness and existing surface. However, quantitative agreement with the experiment is not achieved, since the gigantic SHA of about 12% was measured for a much thicker film of 10 nm (∼40 ML).

IV. CONCLUSION

We investigated the influence of quantum confinement on the skew-scattering contribution to the SHE by means of first-principles calculations. We show that the strength of the penomenon can be tuned by both the impurity position within a metal film and its thickness. For the particular situation of fcc Au(111) films with Pt impurities, the SHA practically does not exceed the bulk value besides the case of adatoms. They can reverse the sign of the SHE in comparison to substitutional impurities and provide a SHA up to 18% for 1 ML noble metal films. The origin of the gigantic SHE is attributed to lacking interband transitions for the one-monolayer films.

*cherschb@mpi-halle.mpg.de

[1]T. Seki, Y. Hasegawa, S. Mitani, S. Takahashi, H. Imamura, S. Maekawa, J. Nitta, and K. Takanashi, Nat. Mater. **7**, 125 (2008).

[2]G. Mihajlović, J. E. Pearson, M. A. Garcia, S. D. Bader, and A. Hoffmann, Phys. Rev. Lett. **103**, 166601 (2009).

[3]G. Y. Guo, S. Maekawa, and N. Nagaosa, Phys. Rev. Lett. **102**, 036401 (2009).

[4]M. Gradhand, D. V. Fedorov, P. Zahn, and I. Mertig, Phys. Rev. Lett. **104**, 186403 (2010).

[5]A. B. Shick, J. Kolorenc, V. Janis, and A. I. Lichtenstein, Phys. Rev. B **84**, 113112 (2011).

[6]B. Gu, I. Sugai, T. Ziman, G. Y. Guo, N. Nagaosa, T. Seki, K. Takanashi, and S. Maekawa, Phys. Rev. Lett. **105**, 216401 (2010).

[7]A. Fert, A. Friederich, and A. Hamzic, J. Magn. Magn. Mater. **24**, 231 (1981).

[8]S. Lowitzer, M. Gradhand, D. Ködderitzsch, D. V. Fedorov, I. Mertig, and H. Ebert, Phys. Rev. Lett. **106**, 056601 (2011).

[9]Y. Niimi, M. Morota, D. H. Wei, C. Deranlot, M. Basletic, A. Hamzic, A. Fert, and Y. Otani, Phys. Rev. Lett. **106**, 126601 (2011).

[10]A. Fert and P. M. Levy, Phys. Rev. Lett. **106**, 157208 (2011).

[11]J. Zabloudil, R. Hammerling, L. Szunyogh, and P. Weinberger, *Electron Scattering in Solid Matter* (Springer-Verlag, Berlin, 2005).

[12]M. Gradhand, M. Czerner, D. V. Fedorov, P. Zahn, B. Y. Yavorsky, L. Szunyogh, and I. Mertig, Phys. Rev. B **80**, 224413 (2009).

[13]I. Mertig, Rep. Prog. Phys. **62**, 237 (1999).

[14]D. V. Fedorov, G. Fahsold, A. Pucci, P. Zahn, and I. Mertig, Phys. Rev. B **75**, 245427 (2007).

[15]F. K. Schulte, Surf. Sci. **55**, 427 (1976).

[16]N. Trivedi and N. W. Ashcroft, Phys. Rev. B **38**, 12298 (1988).

[17]S. Ciraci and I. P. Batra, Phys. Rev. B **33**, 4294 (1986).

[18]M. Gradhand, D. V. Fedorov, P. Zahn, and I. Mertig, Solid State Phenom. **168-169**, 27 (2011).

[19]B. Gu, T. Ziman, G. Y. Guo, N. Nagaosa, and S. Maekawa, J. Appl. Phys. **109**, 07C502 (2011).